25th ABCM International Congress of Mechanical Engineering
October 20-25, 2019, Uberlândia, MG, Brazil

COBEM2019 - 0206
A performance comparison between coupling schemes for poroelasticity

Hermínio T. Honório
herminio@sinmec.ufsc.br
Aideé A. Torres
aideetorres@sinmec.ufsc.br
Bruno Martins
bmartins@sinmec.ufsc.br
Felipe W. Giacomelli
felipe.g@sinmec.ufsc.br
Clovis R. Maliska
maliska@sinmec.ufsc.br
Federal University of Santa Catarina - UFSC

Abstract. *This paper presents a performance comparison between two of the main coupling strategies for poroelasticity problems. In the fully implicit method, the coupling between fluid flow and geomechanical models is implicitly solved in a single system of equations, whereas the fixed-stress split solves these two models separately (two linear systems) in an iterative cycle for each time step. Classical poroelasticity problems are solved in order to assess computational time spent with the two proposed strategies. For the one-dimensional Terzaghi's poroelastic column and the Cryer's sphere, results show that the fully implicit scheme is always faster than the fixed-stress split. However, this time saving decreases with grid refinement.*

Keywords: *poroelasticity, geomechanics, finite volume, fixed-stress split, fully implicit scheme*

1. INTRODUCTION

The theory of poroelasticity is employed for describing a wide variety of problems, such as the mechanical behavior of bone structures (Swan *et al.*, 2003), tumor growth (Roose *et al.*, 2003), water withdrawal (Gambolati *et al.*, 2000), etc. All these problems are composed of a saturated porous matrix subjected to an external load and body forces (usually the gravitational field). These forces are balanced by the solid matrix and the fluid filling its pores, according to Terzaghi's effective stress principle (Terzaghi, 1923). In these problems, the mechanical behavior of the porous structure is coupled with the fluid movement through its pore channels. The reverse is also true, that is, the fluid flow also depends on the porous structure movement. This happens because when the fluid moves, it changes the pore pressure field, which in turn causes a force imbalance in the porous matrix. As a response, the solid matrix deforms in order to reach a new equilibrium state, changing the pore channels and affecting the fluid flow. Therefore, it is clear that the fluid flow model is coupled with the poromechanical model. Although the mathematical coupling between these two models is well defined by Biot's consolidation theory (Biot, 1941), different alternatives are found in the literature for its numerical treatment. The two main coupling strategies are named as *fully implicit coupled* and *iteratively coupled* (Kim *et al.*, 2011a).

In the fully implicit coupling technique, the discretized equations of the fluid flow and geomechanical models are solved simultaneously in the same system of equations, so the coupling between the two models is implicitly solved. The implicit treatment of the coupling provides great robustness and stability to the numerical scheme and the system of equations, for linear problems, needs to be solved only once at each time level. However, due to the dimensions of the linear system, the fully implicit coupling technique can be very time consuming when fine grids are employed. Additionally, it requires a unified framework to be implemented, which excludes the possibility of using different simulators for fluid flow and geomechanical models as often done in the industry and academy (Settari *et al.*, 1998; Cuisiat *et al.*, 1998; Rutqvist *et al.*, 2002; Mainguy and Longuemare, 2002; Huang *et al.*, 2013; Benisch *et al.*, 2013).

As an alternative, iteratively coupled techniques propose the solution of both models separately in order to deal with smaller systems of equations with the expense of performing an iterative cycle for each time level. Usually, the fluid flow model is first solved to determine pressure and the geomechanical model is solved for displacements (fixed-strain and fixed-stress splits, as presented in Kim *et al.* (2011c). Conversely, the drained and undrained splits (Kim *et al.*, 2011b) solves geomechanics first and then the fluid flow model. Whether the geomechanics is solved first or not, both models are separetly solved in an iterative cycle until convergence is reached for each time step. In this manner, although smaller linear systems are built, they have to be repeatedly solved at each time step, which can also have a negative effect in

computational effort. Among these methods, the fixed-stress split has been shown to be the most robust scheme and it is widely applied (Kim *et al.*, 2011a; Mikelić and Wheeler, 2013; White *et al.*, 2016, 2018).

In this work, a comparison, in terms of computational effort (CPU time), is performed between the fully implicit coupled method (FIM) and the fixed-stress splitting scheme. The Element-based Finite Volume Method (EbFVM) is used for obtaining the algebraic representation of the governing partial differential equations. Moreover, unstructured three-dimensional grids are employed. For the comparisons, classical problems of poroelasticy are solved with the two coupling strategies, namely, the Terzaghi's poroelastic problem and the Cryer's sphere.

2. MATHEMATICAL MODEL

Usually, traditional reservoir simulators only consider the geomechanical effects through solid compressibility and porosity variations. However, for coupled geomechanics the rate of volumetric strain plays a key role in the mass conservation equation. By considering a slightly compressible fluid of density ρ and viscosity μ, according to Biot's consolidation theory, the mass balance equation can be written as follows

$$\frac{1}{M}\frac{\partial p}{\partial t} - \nabla \cdot \left[\frac{\mathbf{k}}{\mu} \cdot (\nabla p - \rho \mathbf{g})\right] = -\alpha \frac{\partial \epsilon_v}{\partial t}, \tag{1}$$

where α is the Biot's coefficient, $\mathbf{k}$ is the absolute permeability tensor and $1/M = [\phi c_f + (\alpha - \phi)c_s]$, with ϕ, c_f and c_s respectively being the porosity, fluid and solid compressibility. The volumetric strain is given by the divergence of the displacement vector, that is, $\epsilon_v = \nabla \cdot \mathbf{u}$.

Although Eq. 1 is the usual form for presenting the mass balance equation for pororlasticity, it can be written in an alternative manner that will turn to be useful for the purposes of this work. By recognizing that the volumetric strain is directly proportional to the volumetric effective stress, σ'_v, through the expression $\sigma'_v = K\epsilon_v$, with K being the bulk modulus, and, according to Terzaghi's principle of effective stress, the following relationship holds,

$$\sigma_v = K\epsilon_v - \alpha p \qquad \rightarrow \qquad \epsilon_v = \frac{1}{K}(\sigma_v + \alpha p), \tag{2}$$

where σ_v denotes the total volumetric stress.

By substituting the Eq. 2 into Eq. 1, rearranging the terms and multiplying the resulting equation by αM, the following version of the mass balance equation is obtained

$$\alpha\,(1+\tau)\,\frac{\partial p}{\partial t} - \alpha M \nabla \cdot \left[\frac{\mathbf{k}}{\mu} \cdot (\nabla p - \rho \mathbf{g})\right] + \tau \frac{\partial \sigma_v}{\partial t} = 0, \tag{3}$$

where the new parameter τ is referred to as the *coupling strength* and it is given by,

$$\tau = \frac{\alpha^2 M}{K}. \tag{4}$$

As can be inferred by the name, the coupling strength is a parameter that determines how tight the fluid flow and geomechanics are coupled to each other. For instance, let us consider a very stiff porous matrix with bulk modulus, K, tending to infinity. In this situation, an external load applied to the system will not cause any deformation to the porous matrix, so the fluid flow is not affected by geomechanics. It is easy to see that if $K \rightarrow \infty$, then $\tau \rightarrow 0$ and thus Eq. 3 decouples from the total volumetric stress term. Conversely, a very soft material ($K \rightarrow 0$) increases the coupling strength and consequently the mass balance equation is highly affected by the rock/soil geomechanics.

Finally, the geomechanical model is given by the stress equilibrium equation considering the effective stress tensor $\boldsymbol{\sigma}'$ and the pore pressure p, as proposed by Terzaghi (1923). Moreover, when small strains and the Hookes's law for linear poroelasticity are considered, the stress equilibrium equations can be written in terms of the displacement vector as follows:

$$\nabla \cdot \left[\frac{1}{2}\mathbb{C} : \left(\nabla \mathbf{u} + \nabla \mathbf{u}^T\right) - \alpha p \mathbf{I}\right] = \mathbf{b}^u \tag{5}$$

where $\mathbf{I}$ is a second-order identity tensor, $\mathbf{b}^u$ is a vector representing body forces and $\mathbb{C}$ is a fourth-order tensor representing the stress-strain constitutive relationship.

Equations 1 and 5 compose the system of partial differential equations that governs coupled poroelasticity problems. For proper boundary conditions and initial conditions, this system is solved for obtaining the pressure (p) and displacement $(\mathbf{u})$ fields.

3. NUMERICAL FORMULATION

In this work, the algebraic representation of the governing equations is obtained through the Element-based Finite Volume Method (EbFVM) for spatial discretization and a first-order fully implicity scheme for time discretization. Let us consider a three-dimensional control volume built around a general grid node i, with volume $\Delta\Omega_i$ and bounded by a surface Γ_i, as show in Figure 1. The surface Γ_i is further split into individual faces, each containing an integration point ip with an area vector $\mathbf{s}$ pointing outwards the control volume.

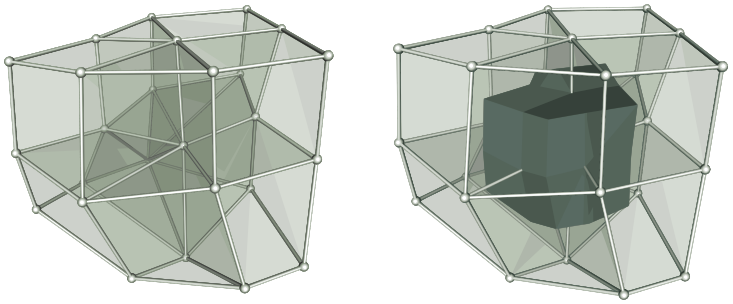

(a) (b)

Figure 1. (a) Unstructured Grid and (b) Control Volume around a grid node.

Equations 1 and 5 are first integrated in time, between t and $t + \Delta t$, and then over the control volume Ω_i. In the sequence, the divergence theorem is recalled in order to transform the volumetric integral of the divergence terms into a surface integral of Γ_i. Finally, the midpoint rule is employed to evaluate the surface integral at the integration points ip belonging to Γ_i, which leads to:

$$\frac{\Delta\Omega_i}{M\Delta t}p_i + \sum_{\mathrm{ip}\in\Gamma_i}\left(\mathrm{Q_{ip}}\mathbf{u}^e - \mathrm{H_{ip}}\mathbf{p}^e\right) = \frac{\Delta\Omega_i}{M\Delta t}p_i^o + \sum_{\mathrm{ip}\in\Gamma_i}\left(\mathrm{Q_{ip}}\mathbf{u}^e\right)^o + b^p \tag{6}$$

$$\sum_{\mathrm{ip}\in\Gamma_i}\left(\mathrm{K_{ip}}\mathbf{u}^e - \mathrm{L_{ip}}\mathbf{p}^e\right) = \mathbf{b}_i^u\Delta\Omega_i \tag{7}$$

In Equation 6, b^p contains the gravitational term and the superscript "^{o}" denotes the variables evaluated at the previous time level t. Additionally, the superscript ^{e} indicates the set of unknowns (pressure or displacements) associated to the vertices of element e containing the integration point ip. Matrices $\mathrm{Q_{ip}}$, $\mathrm{H_{ip}}$ denote linear operators acting on the nodal unknowns to recover the mass flux crossing Γ_i due to solid movement and seepage velocity, respectively. Similarly, terms $\mathrm{K_{ip}}\mathbf{u}^e$ and $\mathrm{L_{ip}}\mathbf{p}^e$ provide the force vectors acting on the control surface due to effective stress $\boldsymbol{\sigma}'$ and to the pore pressure p, respectively. A detailed description of the discretization process to obtain Equations 6 and 7 can be found in Honório *et al.* (2018).

Equations 6 and 7 are obtained for every node of the grid. When grouped together, they compose a linear system of equations of the following form:

$$\begin{bmatrix}-\mathrm{K} & \mathrm{L}\\ \mathrm{Q} & \mathrm{D}\end{bmatrix}\begin{bmatrix}\mathbf{u}\\ \mathbf{p}\end{bmatrix} = \begin{bmatrix}\mathbf{b}^u\\ \mathbf{b}^p\end{bmatrix} \tag{8}$$

where $\mathrm{D} = \mathrm{A} - \mathrm{H}$, with A being a diagonal matrix containing the accumulation terms and H containing terms related to the seepage velocity.

4. COUPLING TECHNIQUES

There are different techniques for solving the linear system of Eq. 8. In this work we focus on the two most common choices for solving coupled poroelasticity problems, namely, the fully implicit scheme and the fixed-stress splitting scheme. Both techniques are presented bellow.

4.1 Fully implicit scheme

The coupling between Equations 6 and 7 can be taken implicitly by solving the hole system of equations as it is presented in Eq. 8. The solution vector at time level $t + \Delta t$ is obtained by multiplying the inverse of the coefficient matrix by the independent vector evaluated at the previous time level t. The time marching procedure is represented in Algorithm 1, where it can be noticed that the complete system of equations has to be inverted (or iteratively solved), which can be an excessively time consuming task for very fine grids. However, once solved, $\mathbf{p}$ and $\mathbf{u}$ simultaneously satisfy both mass and momentum conservation equations, so the algorithm can proceed to the next time level.

Algorithm 1: Algorithm for fully implicit coupling scheme.

Data: $\mathbf{p}^o$, $\mathbf{u}^o$, Δt, t_{initial} and t_{final}

$t \leftarrow t_{\text{initial}}$
while $t < t_{\text{final}}$ **do**
  $\begin{bmatrix}\mathbf{u}\\ \mathbf{p}\end{bmatrix} \leftarrow \begin{bmatrix}-\mathrm{K} & \mathrm{L}\\ \mathrm{Q} & \mathrm{D}\end{bmatrix}^{-1} \begin{bmatrix}\mathbf{b}^u\\ \mathbf{b}^p\end{bmatrix}$
  $\begin{bmatrix}\mathbf{u}\\ \mathbf{p}\end{bmatrix}^o \leftarrow \begin{bmatrix}\mathbf{u}\\ \mathbf{p}\end{bmatrix}$
  $t \leftarrow t + \Delta t$
end

Algorithm 2: Algorithm for fixed-stress splitting scheme.

Data: $\mathbf{p}^o$, $\mathbf{u}^o$, Δt, t_{initial} and t_{final}

$t \leftarrow t_{\text{initial}}$
while $t < t_{\text{final}}$ **do**
  $\mathbf{p}^{k-1} \leftarrow \mathbf{p}^o$; $\mathbf{u}^{k-1} \leftarrow \mathbf{u}^o$
  while error $<$ tol **do**
    $\mathbf{p}^k \leftarrow (\mathrm{D}+\mathrm{B})^{-1}\left(\mathbf{b}^p - \mathrm{Q}\mathbf{u}^{k-1} + \mathrm{B}\mathbf{p}^{k-1}\right)$
    $\mathbf{u}^k \leftarrow \mathrm{K}^{-1}\left(\mathrm{L}\mathbf{p}^k - \mathbf{b}^u\right)$
    error $\leftarrow \mathrm{abs}(\max(p^k - p^{k-1}))$
    $\mathbf{p}^{k-1} \leftarrow \mathbf{p}^k$; $\mathbf{u}^{k-1} \leftarrow \mathbf{u}^k$
  end
  $\mathbf{p}^o \leftarrow \mathbf{p}^k$; $\mathbf{u}^o \leftarrow \mathbf{u}^k$; $t \leftarrow t + \Delta t$
end

4.2 Fixed-stress split

Iterative coupling schemes are employed in order to avoid dealing with the full coefficient matrix. Instead, they split the mass and momentum equations and solve them sequentially until convergence is reached for each time level. The fixed-stress scheme is a splitting technique first proposed by Kim *et al.* (2011c), in which flow and geomechanical models are iteratively solved for each time step, while keeping the total volumetric stress (σ_v) fixed from one iteration to another. For splitting both equations, ϵ_v must be explicitly evaluated in the mass conservation equation. Let's define the current iteration at each time step level as k and the explicit volumetric strain as $\bar{\epsilon}_v$. The natural choice is to use the displacement vector of the previous iteration for evaluating the explicit volumetric strain ($\bar{\epsilon}_v = \epsilon_v^{k-1}$), thus freezing the volumetric strain from one iteration to another (fixed-strain split). For the fixed-stress split, however, the total volumetric stress σ_v is freezed at each iteration. This is possible by recalling that $\sigma_v' = K\epsilon_v$, which allows to explicitly evaluate the effective volumetric stress, $\bar{\sigma}'$, as follows,

$$\bar{\epsilon}_v = \frac{\bar{\sigma}_v'}{K} = \frac{1}{K}(\sigma_v^{k-1} + \alpha p^k) = \frac{1}{K}\left(K\epsilon_v^{k-1} - \alpha p^{k-1} + \alpha p^k\right) \quad \rightarrow \quad \bar{\epsilon}_v = \epsilon_v^{k-1} - \frac{\alpha}{K}p^{k-1} + \frac{\alpha}{K}p^k \tag{9}$$

By substituting Eq. 9 into Eq. 1, the mass conservation equation for the fixed-stress splitting scheme can be written as follows:

$$\left(\frac{1}{M} + \frac{\alpha^2}{K}\right)\frac{\partial p^k}{\partial t} - \nabla\cdot\left(\frac{\mathbf{k}}{\mu}\cdot\nabla p^k\right) = \frac{\alpha^2}{K}\frac{\partial p}{\partial t}^{k-1} - \alpha\frac{\partial \epsilon_v}{\partial t}^{k-1} - \nabla\cdot\left(\frac{\rho\mathbf{k}}{\mu}\cdot\mathbf{g}\right) \tag{10}$$

The discretization process of Eq. 10 is exactly the same as presented before. The resulting system of equations for mass conservation then takes the form below:

$$(\mathrm{D}+\mathrm{B})\,\mathbf{p}^k = \mathbf{b}^p - \mathrm{Q}\mathbf{u}^{k-1} + \mathrm{B}\mathbf{p}^{k-1} \tag{11}$$

$$\mathbf{p}^k = (\mathrm{D}+\mathrm{B})^{-1}\left(\mathbf{b}^p - \mathrm{Q}\mathbf{u}^{k-1} + \mathrm{B}\mathbf{p}^{k-1}\right) \tag{12}$$

where matrix B is a diagonal matrix containing terms α^2/K. The solution procedure thus require an internal iterative cycle for each time step of the simulation. The algorithm for the fixed-stress splitting scheme can be represented as in Algorithm 2. In spite of performing an internal iterative cycle, in which flow and geomechanical models are solved, only matrices K and $(\mathrm{D}+\mathrm{B})$ have to be inverted, which are quite smaller than the full coefficient matrix of Eq. 8.

5. RESULTS

The numerical schemes presented before are implemented in a C++ in-house library called *EFVLib2018*, which was specially developed for implementing element-based finite volume formulations. For dealing with the linear systems we employ the *Portable, Extensible, Toolkit for Scientific Computation* (Abhyankar *et al.*, 2018). The results presented below were obtained with CPU running on a Intel(R) Core(TM) i7-4770 CPU @ 3.40GHz with 16,3 GB of RAM.

The rationale of the comparisons performed in this paper is to identify which variables affect the total CPU time and how they affect it. Evidently, the CPU time is directly linked with the linear system size, so the number of nodal points in the grid must be one of the variables considered here. Although we expect the computational effort to increase with grid refinement, it is not readily clear how it affects both coupling strategies. Another variable to be considered is the coupling

strength, which certainly affects the number of internal iterations of the fixed-stress scheme but it is not totally clear, in principle, whether or not it causes any impact on the fully implicit scheme.

Finally, for a given final time we want to know how the time step size impacts CPU time for both strategies. However, as we modify the coupling strength the time scales involved automatically change as well. In order to avoid this problem, we employ a dimensionless time given by,

$$t_d = \frac{c_v t}{h^2}, \tag{13}$$

where t denotes the time in real dimension, h is the characteristic length and c_v is the consolidation coefficient, estimated as follow

$$c_v = \frac{k}{\gamma_f(\alpha^2 m_v + S)} \tag{14}$$

where, k is the permeability, γ_f is the specific weight of the fluid, α is the Biot's coefficient, S is the Storativity given by $S = \phi c_f + (\alpha - \phi)c_s$ and m_v is the confined compressibility of the porous medium, given by

$$m_v = \frac{1}{K + \frac{4}{3}G}. \tag{15}$$

In the following examples, the dimensionless total time is always $t_{\text{final}} = 3,31 \times 10^{-7}$ and three time step sizes are $9,93 \times 10^{-9}$, $3,31 \times 10^{-10}$ and $3,31 \times 10^{-11}$.

5.1 Therzaghi's Poroelastic Column

Therzaghi's poroelastic column is one of the most simple problems of poroelasticity. This problem consists of a one-layered column with impermeable laterals boundaries with no lateral movements and a fixed bottom boundary also impermeable. The upper boundary is drained ($\delta p = 0$) and a compressive load is applied on it. The problem is illustrated in Fig. 2(a).

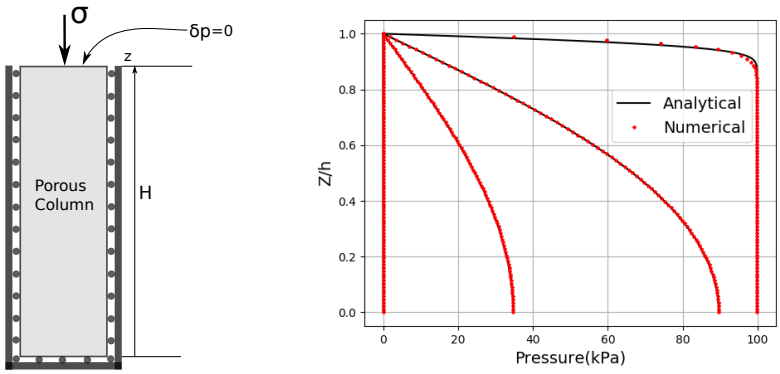

(a) (b)

Figure 2. (a) Therzahi's poroelastic column and (b) Analytical and numerical solutions for different time steps.

For this problem, a 6 meters tall with 1m^2 of cross-section area is employed. A compressive load of 100kPa is applied on the top boundary. As mentioned before, three different dimensionless time step sizes and a fixed dimensionless final time are used in this problem. For validation purposes, the numerical solution is plotted against the analytical solution in Fig. 2(b) (the analytical solution for this problem can be found in several works, e.g.Verruijt (2016)). .

Figure 3 shows three different plots, one for each time step size. Each graphic represents the CPU time increase for progressively refined grids and for different coupling strengths. We must emphasize that the simulations revealed that the fully implicit scheme is totally independent of the coupling strength, which is why only one curve is plotted for this method. In contrast to the fully implicit scheme, the fixed-stress scheme is highly affected by the coupling strength. It is possible to notice that when the first three coupling strengths are compared a significant increase of CPU Time is perceived. The CPU time curve for the fixed-stress is almost the same for the coupling strengths of 46,2 and 1.040,4.

For the first time step size, Figure 3, the largest CPU Time was 1.750 s for a coupling strength of 1040,4 and a grid with 22.784 nodes for the fixed-stress scheme, whereas the fully implicit scheme with the same grid and the same coupling strength only takes 367 s to solve the linear system. As it can be seen in Figure 3, the behavior is the same for the others time steps, that is, the largest CPU time is always obtained for the higher coupling strength.

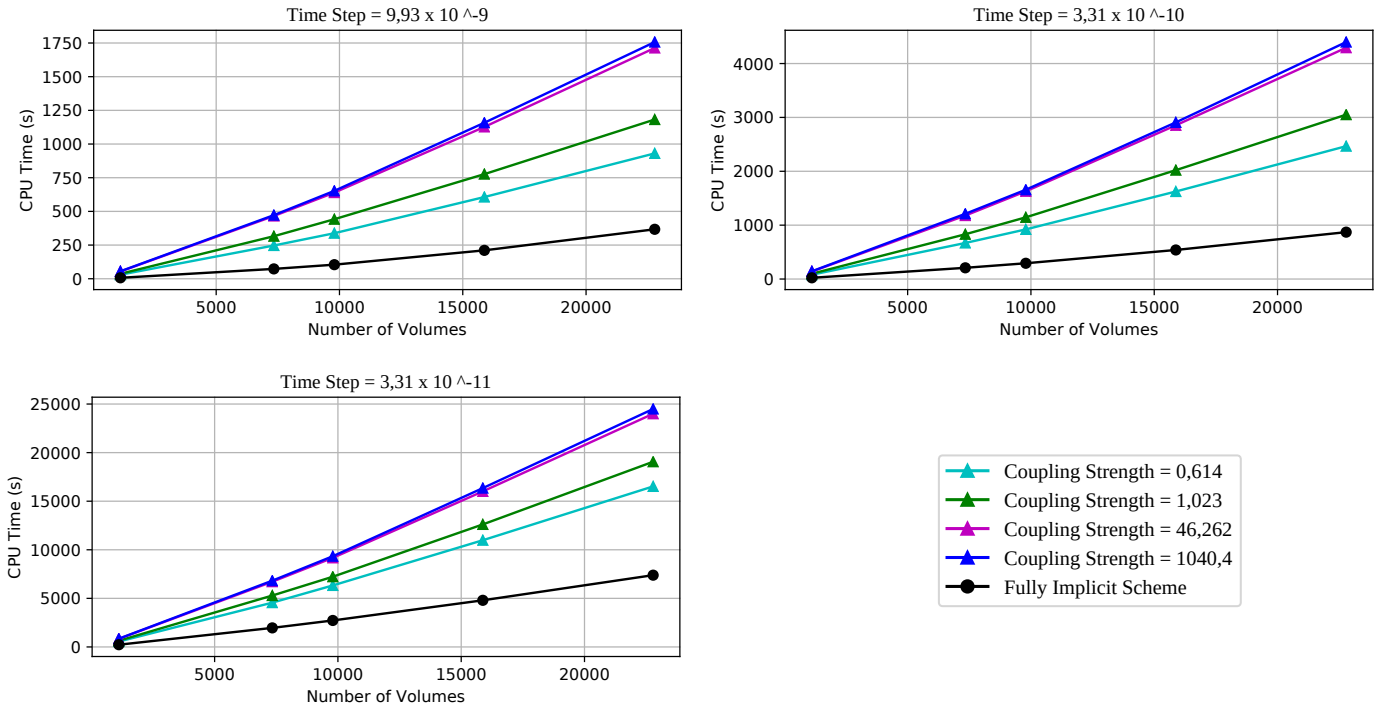

Figure 3. Performance results of Terzaghi's problem.

Another important detail is the difference between the third, $46,262$, and the fourth, $1.040,4$, coupling strength when the fixed-stress is being used. There is almost no difference between the these curves, independently of the time step size. A careful look at this results suggests that the increase in the CPU time due to an increase of the coupling strength is not linear. In order to highlight this behavior, we freeze a time step size and plot the CPU time against the coupling strength for different grid sizes. The results are shown in Fig. 4 and they reveal that the fixed-stress scheme is only dependent on the coupling strength until certain value.

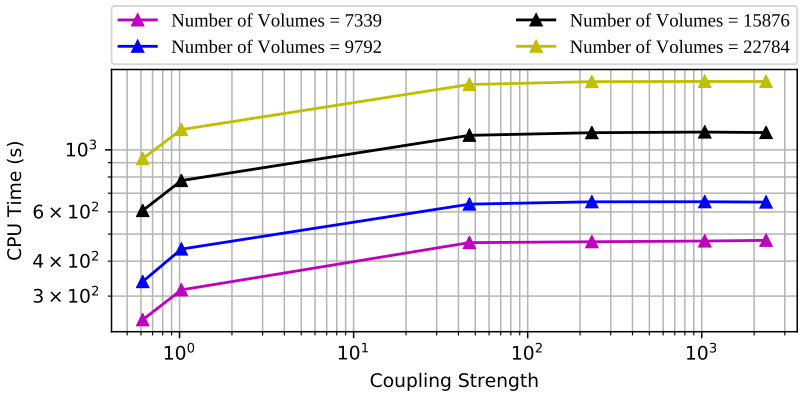

Figure 4. Behavior of the CPU Time with the coupling strength for the Terzaghi's problem.

So far, the results have shown that the fully implicit scheme is always faster than the fixed-stress scheme. A useful analyzes is to evaluate the percentage of CPU time reduction (speedup) provided by the fully implicit scheme in comparison with the fixed-stress scheme for progressively refined grids. This result is shown in Fig. 5 for different coupling strengths. As it can be verified, in general, the larger the time step size is, the larger the speedup observed. Additionally, the speedup decreases with grid refinement and with the coupling strength.

5.2 Cryer's Sphere

In this problem, a spherical poroelastic material is fully saturated and a compressive load of magnitude q is applied on the surface of the sphere, which is undrained at first. As a result, a constant pressure p^0 and volumetric strain ϵ_v establishes in entire domain. From this situation, the surface of the sphere suddenly opens for the fluid flow ($\delta p = 0$), which causes a pressure front to travel towards its center. A representation of the boundary condition and the domain is

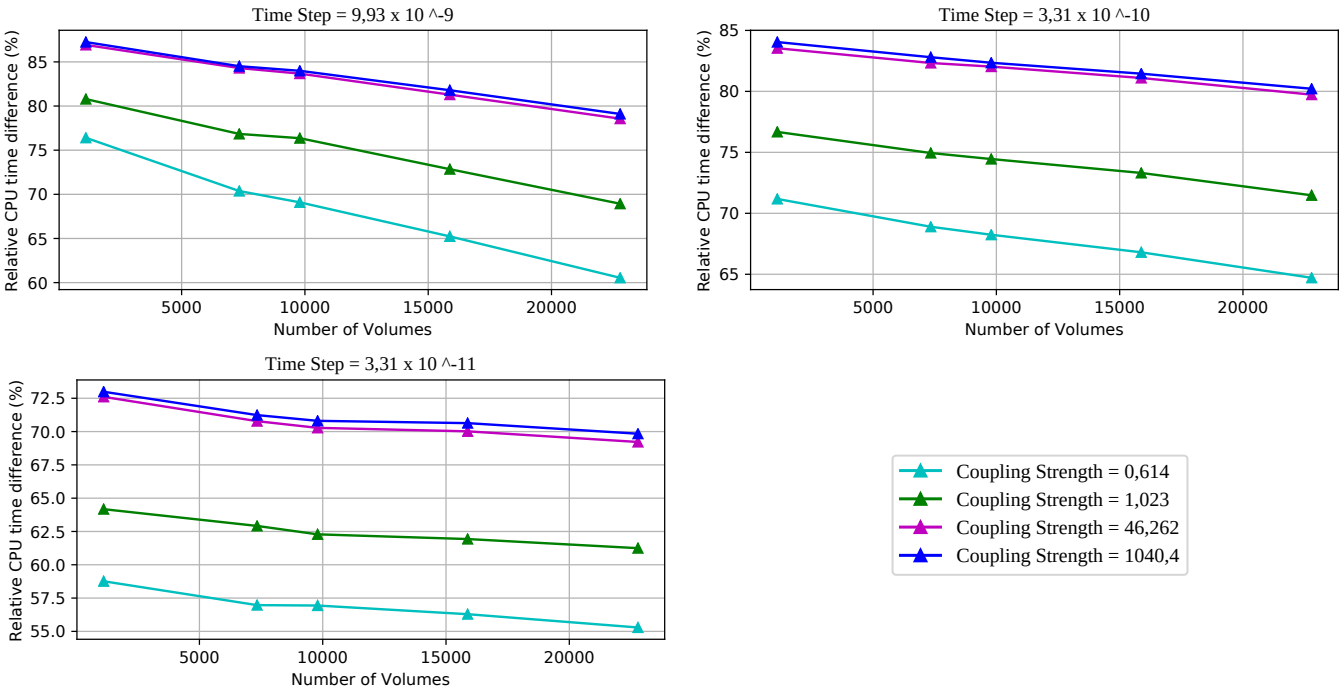

Figure 5. Relative CPU time difference between the two coupling scheme with respect to the grid refinement for Terzaghi's Problem.

shown in Fig. 6(a). The combination of the boundary conditions with the spherical domain provides the conditions for the Mandel-Cryer effect to appear. This phenomenon is characterized by a pressure increase above the initial pressure p^0 in the center of the sphere. This pressure increase tends to dissipate as the pressure front reaches the center of the domain. The analytical solution for the pressure at the center is plotted against the numerical results in Fig. 6(b). The Mandel-Cryer effect is a clear evidence of the coupling between fluid flow and geomechanics, which cannot be observed in Terzaghi's poroelastic column.

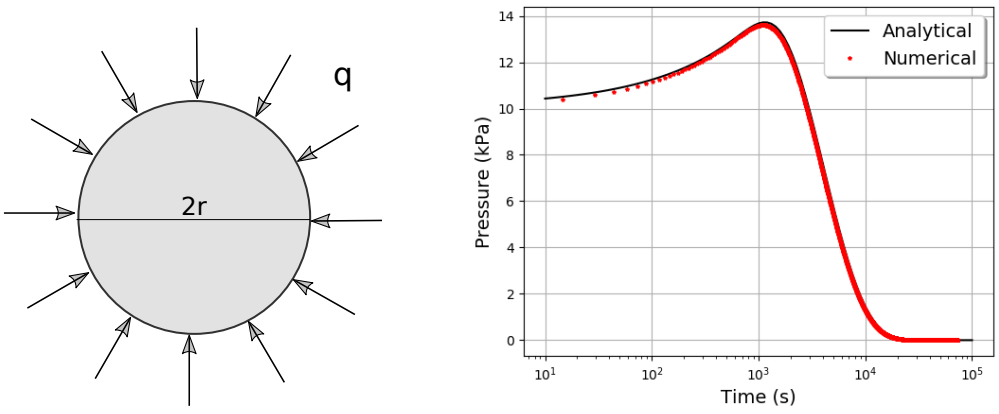

(a) (b)

Figure 6. (a) Cryer's sphere and (b) Analytical and numerical comparison.

The Cryer's sphere is solved with a set of progressively refined grids and different coupling strengths. The dimensionless final time and time step sizes are the same as the ones employed in the poroelastic column. Fig. 7 shows the CPU times obtained for both coupling schemes. As evidenced in Fig. 7, the results are very similar to those obtained in Terzaghi's problem. The fully implicit scheme presented similar CPU times for all the coupling strengths and, therefore, the results for this scheme are represented in a single curve. The major difference between the CPU times are observed in the first three coupling strength, after that the CPU time are practically the same. Once again, the largest CPU time appears in the case with the smallest time step size is used with the largest coupling strength for the fixed-stress scheme.

A closer look at Fig. 7 reveals that the CPU time of the fixed-stress scheme increases with the coupling strength, but

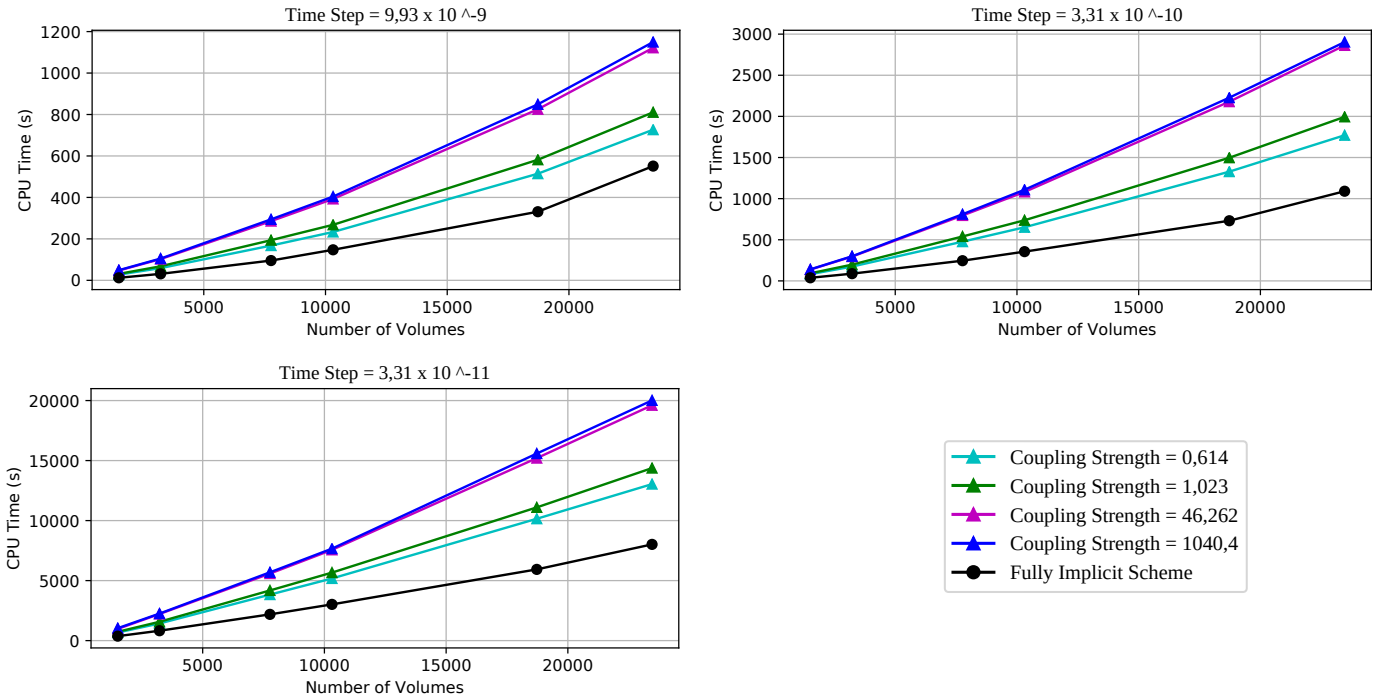

Figure 7. Performance results of Cryer's sphere.

this increment becomes negligible beyond certain values of τ. In order to highlight this point, in Fig. 8 we plot the CPU time of the fixed-stress scheme for increasing values of coupling strength. The dimensionless time step size in this case was chosen to be $9,93 \times 10^{-9}$. As it can be verified, after $\tau = 100$ the performance of the fixed-stress scheme becomes almost independent of the coupling strength, which was also observed for the Terzaghi's problem.

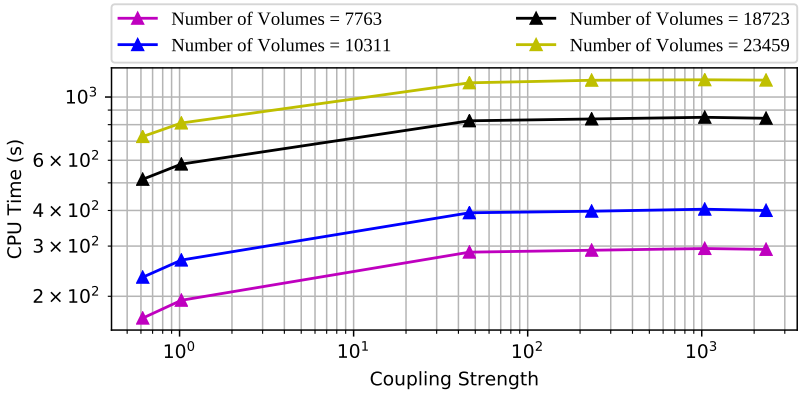

Figure 8. Behavior of the CPU Time with the coupling strength for the Cryer's sphere.

The fully implicit scheme presented the best performance for the Cryer's sphere in all situations, as it can be verified in Fig. 7. The speedup provided by this coupling technique, however, decreases with grid refinement, as shown in Fig. 9. This result suggests that, for sufficiently large grids, the CPU time required by both coupling techniques tends to be the same. In other words, the speedup tends to zero. We can also point out that the maximum speedup of the fully implicit scheme for the Cryer's sphere is smaller than the one obtained for the Terzaghi's poroelastic column, shown in Fig. 5.

6. CONCLUSIONS

This paper presents a systematic comparison between the two main coupling schemes for solving coupled poroelasticity problems, namely the fully implicit and the fixed-stress splitting schemes. Despite both strategies being recognized to be unconditionally stable, the fixed-stress scheme is the most commonly used as it is easier to implement and it allows the coupling between different simulators for fluid flow and geomechanics. The performance of this two techniques are assessed by analyzing the resulting CPU time in different situations. The classical poroelastic column of Terzaghi and the Cryer's sphere are numerically solved with both coupling strategies. Additionally, we investigate the sensibility of these

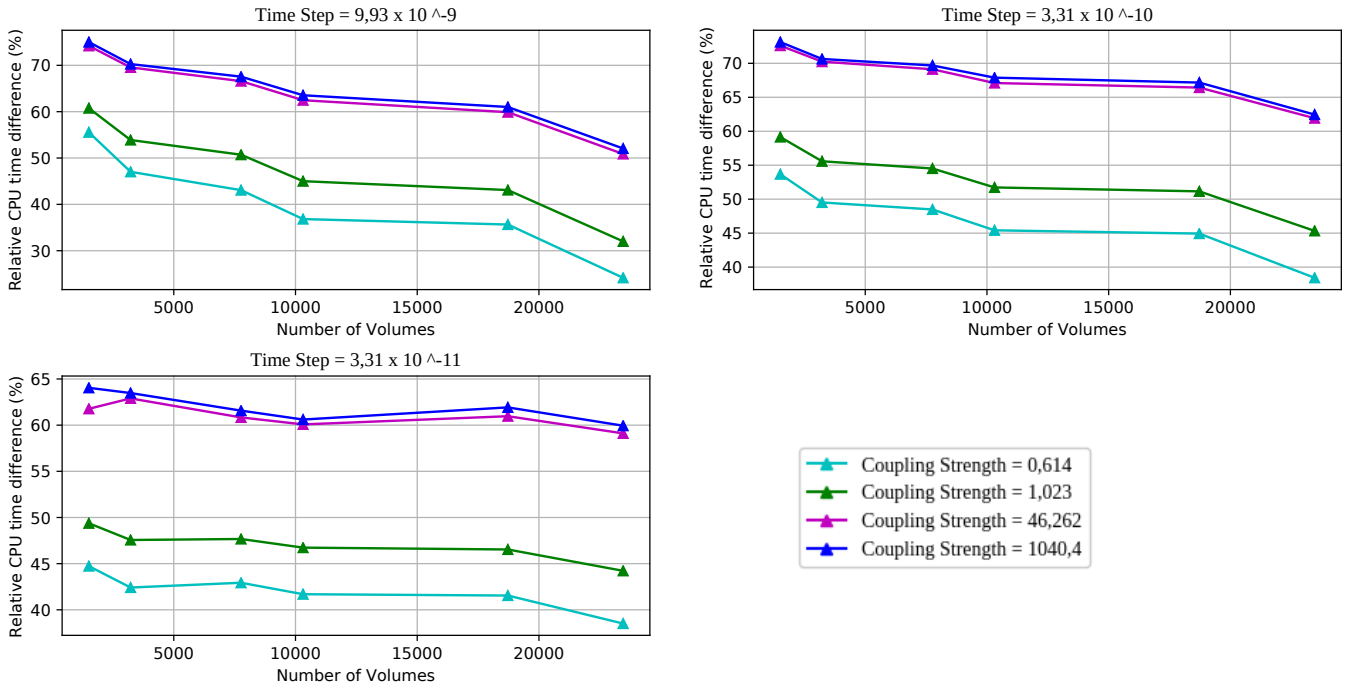

Figure 9. Relative CPU time difference between the two coupling scheme with respect to the grid refinement for Cryer's sphere.

two techniques with the time step size, coupling strength and grid refinement.

The results presented in this paper show that the fully implicit scheme always present the best performance in terms of CPU time. This show that, in the fixed-stress scheme, dealing with smaller linear systems does not pay off, since the time spent to perform the iterative cycle prevails. Additionally, the fully implicit scheme does not depend on the coupling strength. The fixed-stress scheme, on the other hand, is significantly affected by this parameter.

The choice of the time step size seems to have some influence on the speedup of the fully implicit scheme compared to the fixed-stress. According to the results presented, the speedup decreases faster with grid refinement for larger time step sizes. The speedup graphics also show that the fully implicit scheme is strongly recommended for highly coupled problems. For small values of coupling strength and very fine grids, the CPU time spent by both techniques tends to be the same.

It is important to stress that, in spite of the results shown in this paper, the fixed-stress scheme has some important aspects that deserve credit. First of all, this technique can be implemented when different simulators are to be used simultaneously. In this situation, the fully implicit scheme is almost impossible to be implemented. Moreover, the coefficient matrix resulting from the fully implicit scheme is prone to suffer from ill-conditioning, which require the use of *ad-hoc* preconditioners in order to prevent divergence. The linear systems resulting from splitting schemes, as the fixed-stress, are always well conditioned and thus easier to solve. The performance in terms of CPU time is important, but there are other aspects that also have to be taken into account when choosing a coupling technique.

7. ACKNOWLEDGEMENTS

This paper has been partially supported by Petrobras within project number 5850.010924.18.9, entitled "Malhas Tridimensionais Híbridas para a Solução do Problema Acoplado Fluxo-Geomecânica", within "Rede Temática GEOMEC".

8. REFERENCES

Abhyankar, S., Brown, J., Constantinescu, E.M., Ghosh, D., Smith, B.F. and Zhang, H., 2018. "Petsc/ts: A modern scalable ode/dae solver library". *arXiv preprint arXiv:1806.01437*.

Benisch, K., Graupner, B. and Bauer, S., 2013. "The coupled opengeosys-eclipse simulator for simulation of co2 storage–code comparison for fluid flow and geomechanical processes". *Energy Procedia*, Vol. 37, pp. 3663–3671.

Biot, M.A., 1941. "General theory of three-dimensional consolidation". *Journal of applied physics*, Vol. 12, No. 2, pp. 155–164.

Cuisiat, F., Gutierrez, M., Lewis, R., Masters, I. *et al.*, 1998. "Petroleum reservoir simulation coupling flow and deformation". In *European Petroleum Conference*. Society of Petroleum Engineers.

Gambolati, G., Teatini, P., Baú, D. and Ferronato, M., 2000. "Importance of poroelastic coupling in dynamically active aquifers of the po river basin, italy". *Water Resources Research*, Vol. 36, No. 9, pp. 2443–2459.

Honório, H.T., Maliska, C.R., Ferronato, M. and Janna, C., 2018. "A stabilized element-based finite volume method for poroelastic problems". *Journal of Computational Physics*, Vol. 364, pp. 49–972.

Huang, H., Wattenbarger, R.C., Gai, X., Brown, W.P., Hehmeyer, O.J., Wang, J. and Long, T.A., 2013. "Using a fully coupled flow and geomechanical simulator to model injection into heavy oil reservoirs". *International Journal for Numerical Methods in Fluids*, Vol. 71, No. 6, pp. 671–686.

Kim, J., Tchelepi, H.A. and Juanes, R., 2011a. "Stability, accuracy and efficiency of sequential methods for coupled flow and geomechanics". *Society of Petroleum Engineers*, Vol. 16, No. 2.

Kim, J., Tchelepi, H.A. and Juanes, R., 2011b. "Stability and convergence of sequential methods for coupled flow and geomechanics: Drained and undrained aplits". *Computer Methods in Applied Mechanics and Engineering*, Vol. 200, pp. 2094–2116.

Kim, J., Tchelepi, H.A. and Juanes, R., 2011c. "Stability and convergence of sequential methods for coupled flow and geomechanics: Fixed-stress and fixed-strain aplits". *Computer Methods in Applied Mechanics and Engineering*, Vol. 200, pp. 1591–1606.

Mainguy, M. and Longuemare, P., 2002. "Coupling fluid flow and rock mechanics: formulations of the partial coupling between reservoir and geomechanical simulators". *Oil & Gas Science and Technology*, Vol. 57, No. 4, pp. 355–367.

Mikelić, A. and Wheeler, M.F., 2013. "Convergence of iterative coupling for coupled flow and geomechanics". *Computational Geosciences*, Vol. 17, No. 3, pp. 455–461.

Roose, T., Netti, P.A., Munn, L.L., Boucher, Y. and Jain, R.K., 2003. "Solid stress generated by spheroid growth estimated using linear poroelasticity model". *Microvascular Research*, Vol. 66, pp. 637–652.

Rutqvist, J., Wu, Y.S., Tsang, C.F. and Bodvarsson, G., 2002. "A modeling approach for analysis of coupled multiphase fluid flow, heat transfer, and deformation in fractured porous rock". *International Journal of Rock Mechanics and Mining Sciences*, Vol. 39, No. 4, pp. 429–442.

Settari, A., Mourits, F. *et al.*, 1998. "A coupled reservoir and geomechanical simulation system". *Spe Journal*, Vol. 3, No. 03, pp. 219–226.

Swan, C.C., Lakes, R.S., Brand, R.A. and Stewart, J.K., 2003. "Micromechanically based poroelastic modeling of fluid flow in haversian bone". *Journal of Biomechanical Engineering*, Vol. 32, pp. 579–606.

Terzaghi, K., 1923. "Die berechnung der durchlassigkeitsziffer des tones aus dem verlauf der hydrodynamischen spannungsercheinungen". *Sitz. Akad. Wissen. Wien. Math. Naturwis*, Vol. 2a, pp. 125–128.

Verruijt, A., 2016. *Theory and problemns of poroelasticity*, Vol. 1. Delt University of Technology.

White, J.A., Castelletto, N., Klevtsov, S., Bui, Q.M., Osei-Kuffuor, D. and Tchelepi, H.A., 2018. "A two-stage preconditioner for multiphase poromechanics in reservoir simulation". *arXiv preprint arXiv:1812.05540*.

White, J.A., Castelletto, N. and Tchelepi, H.A., 2016. "Block-partitioned solvers for coupled poromechanics: A unified framework". *Computer Methods in Applied Mechanics and Engineering*, Vol. 303, pp. 55–74.

9. RESPONSIBILITY NOTICE

The authors are the only responsible for the printed material included in this paper.